Engraftment of human nasal olfactory stem cells restores neuroplasticity in mice with hippocampal lesions

Emmanuel Nivet,[1,2] Michel Vignes,[3] Stéphane D. Girard,[1,2] Caroline Pierrisnard,[1] Nathalie Baril,[1] Arnaud Devèze,[4] Jacques Magnan,[4] Fabien Lanté,[3] Michel Khrestchatisky,[2] François Féron,[2,5] and François S. Roman[1]

[1]Laboratoire de Neurobiologie des Processus Mnésiques, CNRS UMR-6149, Aix-Marseille Université; IFR Sciences du Cerveau et de la Cognition, Marseille, France. [2]Neurobiologie des Interactions Cellulaires et Neurophysiopathologie, CNRS UMR-6184, Faculté de Médecine, Aix-Marseille Université; IFR Jean Roche, Marseille, France. [3]Stress Oxydant et Neuroprotection, CNRS UMR-5247, Université de Montpellier 1 et 2; IBMM, Montpellier, France. [4]Département ORL, Hôpital Universitaire Nord, AP-HM, Marseille, France. [5]Centre d'Investigations Cliniques en Biothérapie CIC-BT 510, AP-HM — Institut Paoli Calmettes — Inserm, Aix-Marseille Université, Marseille, France.

Stem cell–based therapy has been proposed as a potential means of treatment for a variety of brain disorders. Because ethical and technical issues have so far limited the clinical translation of research using embryonic/fetal cells and neural tissue, respectively, the search for alternative sources of therapeutic stem cells remains ongoing. Here, we report that upon transplantation into mice with chemically induced hippocampal lesions, human olfactory ecto–mesenchymal stem cells (OE-MSCs) — adult stem cells from human nasal olfactory lamina propria — migrated toward the sites of neural damage, where they differentiated into neurons. Additionally, transplanted OE-MSCs stimulated endogenous neurogenesis, restored synaptic transmission, and enhanced long-term potentiation. Mice that received transplanted OE-MSCs exhibited restoration of learning and memory on behavioral tests compared with lesioned, nontransplanted control mice. Similar results were obtained when OE-MSCs were injected into the cerebrospinal fluid. These data show that OE-MSCs can induce neurogenesis and contribute to restoration of hippocampal neuronal networks via trophic actions. They provide evidence that human olfactory tissue is a conceivable source of nervous system replacement cells. This stem cell subtype may be useful for a broad range of stem cell–related studies.

Introduction

Repairing the central nervous system is a scientific challenge prompting innovative strategies. A few brain areas have the potential to grow or shrink according to cognitive demands of the environment (1), and acute insults stimulate adult neurogenesis (2). However, resident neuron factories, sustained by neural stem cell niches, usually fail to compensate for the deleterious consequences of severe trauma or neurodegenerative diseases (3, 4). Therefore, exogenous cell therapy has been proposed as an attractive alternative for treating a variety of neurological diseases (5). Cellular transplantation approaches to replace dead cells and/or to act as a neuroprotective agent have been developed over the past 2 decades. The success of such therapeutic treatment fundamentally hinges on the choice of cell type. Several stem and progenitor cell types have been proposed for the treatment of brain injuries. Mouse and human neural stem cells or progenitors transplanted in experimental models of inducible hippocampal neuronal loss (6), Alzheimer disease (7), and aging (8) have shown great promises by significantly improving cognitive functions. Similarly, embryonic stem cells or progenitors are able to rescue cognitive impairment through transplantation in various models (9–11). Although controversial, clinical trials have provided the "proof of principle" that cell transplantation in the brain could be envisaged as a powerful means of treatment for future regenerative medicine (12–14). However, the ethical and technical issues associated with neural and embryonic/fetal (stem) cells have boosted strategies based on autologous grafting of adult peripheral stem cells.

Among the potential stem cell candidates, olfactory lamina propria stem cells, sited in nervous tissue, stand as a promising multipotent contender (15–17). The olfactory mucosa is a permanently self-renewing nervous tissue, even in elderly persons, which harbors a variety of cells supporting both its normal function and its regenerative capacity (18). Olfactory ensheathing cells, involved in axonal outgrowth guidance, have already been described as a valid tool to promote neuroplasticity after brain transplantation (19). Thus, diverting cells of the highly plastic peripheral olfactory system toward a poorly self-renewing area appears as a potential means of treatment of the injured nervous system. Recently, a new resident stem cell type in the olfactory lamina propria was highlighted (16, 17). We characterized this stem cell as a member of the mesenchymal stem cell superfamily displaying neurogenic properties (17) and named it *olfactory ecto–mesenchymal stem cell* (OE-MSC). As stem cells, these cells combine a neural crest origin, high versatility, and an advantageous localization. Indeed, the nasal lamina propria is an easily accessible tissue that can be harvested in every individual under local anesthesia, and OE-MSCs could thus be used for autologous transplantation. Altogether, these singular properties could overcome all the concerns that are usually encountered with most other stem cell types. In the present study, we evaluated their therapeutic potential in an animal model of excitotoxically induced

Authorship note: François Féron and François S. Roman contributed equally to this work.

Conflict of interest: The authors have declared that no conflict of interest exists.

Citation for this article: *J Clin Invest.* 2011;121(7):2808–2820. doi:10.1172/JCI44489.

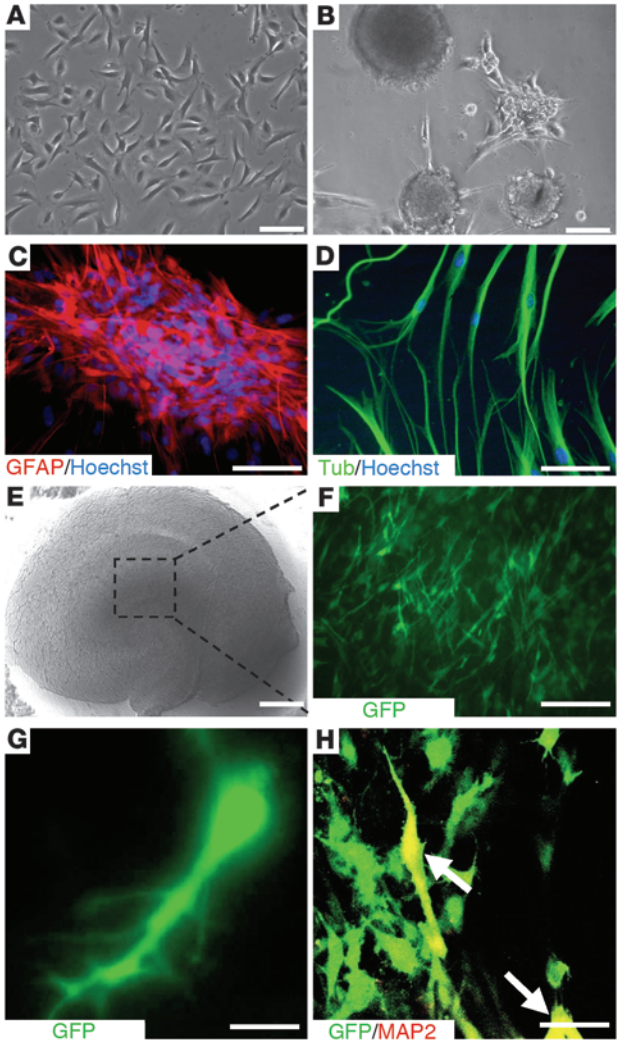

Figure 1
In vitro assessment of neurogenic characteristics of OE-MSCs. Olfactory stem cells (**A**) gave rise to spherical clusters (**B**), expressing the GFAP neural stem cell marker (**C**), when grown in appropriate medium. Cells from spheres were then allowed to differentiate into neurons expressing the III–β-tubulin neuron marker (**D**). Freshly prepared mouse hippocampal slices were cultivated on culture insert (**E**) and loaded with sphere-derived GFP$^+$ OE-MSCs (**F**). 3 weeks after culture at the air-liquid interface, some GFP$^+$ OE-MSCs (green) adopted a neuron-like shape (**G**) and gave rise to MAP_2-expressing neurons (**H**, white arrows). Scale bars: 100 μm (**A**, **B**, **C**, and **D**); 500 μm (**E**); 200 μm (**F**); 20 μm (**G**); 50 μm (**H**).

cell death that closely mimics the effects of an ischemic/hypoxic injury targeting the hippocampus.

The hippocampus is a vulnerable structure (20), located in the medial temporal lobe, that plays a central role in cognitive processes. Hippocampal neuron losses, consecutive to trauma, intoxication, or age-related diseases, induce learning and memory deficits (21, 22). At the molecular level, a dramatic cell death is observed in patients with Alzheimer disease (23) or after an ischemic episode (24). Here we show in a brain-injured mouse model that transplantation of human OE-MSCs enables partial reconstitution of damaged hippocampus. Importantly, engraftment of human OE-MSCs into mouse lesioned hippocampi holds therapeutic value: exogenous stem cells migrate toward the inflamed areas, exhibit in situ neuronal differentiation, stimulate endogenous neurogenesis, restore defective learning and memory abilities, and enhance physiological function (i.e., long-term potentiation [LTP]). Interestingly, we observe similar findings when OE-MSCs are transplanted in the cerebrospinal fluid. Together, our results pave the way for clinical studies based on autologous grafts of nasal olfactory stem cells in patients with posttraumatic memory loss, similarly to what we have done with nasal olfactory ensheathing cells in paraplegic patients (25, 26).

Results

Hippocampal substrate induces in vitro neuronal differentiation of neurogenic human OE-MSCs

OE-MSCs are located within the olfactory lamina propria beneath the olfactory basal lamina. Transcript and membrane protein analyses have shown that OE-MSCs are closely related to bone marrow mesenchymal stem cells (BM-MSCs), but exhibit a high-level expression of genes involved in neurogenesis when compared with BM-MSCs (17). In vitro and under appropriate culture conditions, OE-MSCs are prone to give spheres expressing Nestin, glial fibrillary acid protein (GFAP), and polysialylated neural cell adhesion molecule (PSA-NCAM) markers (16, 17), which are also strongly expressed in neural stem cells (Figure 1, A–C). Moreover, OE-MSCs are found to express III–β-tubulin (Figure 1D) and can be differentiated into MAP2 neuronal cells (17).

In a proof-of-principle experiment, we determined whether, as previously described with mesenchymal stem cells (27), the hippocampus could provide a suitable environment for in vitro neural differentiation of human OE-MSCs. Dissociated sphere-derived OE-MSCs, constitutively expressing GFP, were laid on the top of freshly prepared mouse hippocampal slices cultivated on inserts (Figure 1, E and F). Three weeks after grafting, we observed that surviving GFP$^+$ transplanted cells were still on the top of organotypic hippocampal cultures and some of them (nonquantified) displayed an interneuron-like morphology (Figure 1G) and/or expressed MAP2 mature neuronal markers (Figure 1H). Not a single GFAP-expressing cell was ever found within the exogenous cell population. Some grafted human OE-MSCs exhibited electrophysiological properties consistent with immature neurons (data not shown). With these encouraging in vitro results in hand, we chose to graft OE-MSCs into an in vivo mouse model of ibotenic acid–lesioned hippocampus.

Human OE-MSCs restore learning and memory after transplantation in injured hippocampus

For this first series of experiments, 3 major choices were made: (a) memory dysfunction was induced by provoking cell death within the hippocampal cornu ammonis (CA) and dentate gyrus (DG) layers using ibotenic acid, an excitotoxic NMDA agonist (28); (b) all GFP$^+$ OE-MSCs were derived from a single stem cell originating from a sphere and grafted within the lesion site; and (c) no immunosuppressant was delivered to mice transplanted with human stem cells, in order to avoid a putative confounding factor.

Twenty-four hours after hippocampal lesion was induced, brains were screened using MRI (Figure 2, A and B) and animals without signs of bilateral inflammation within the hippocampus were

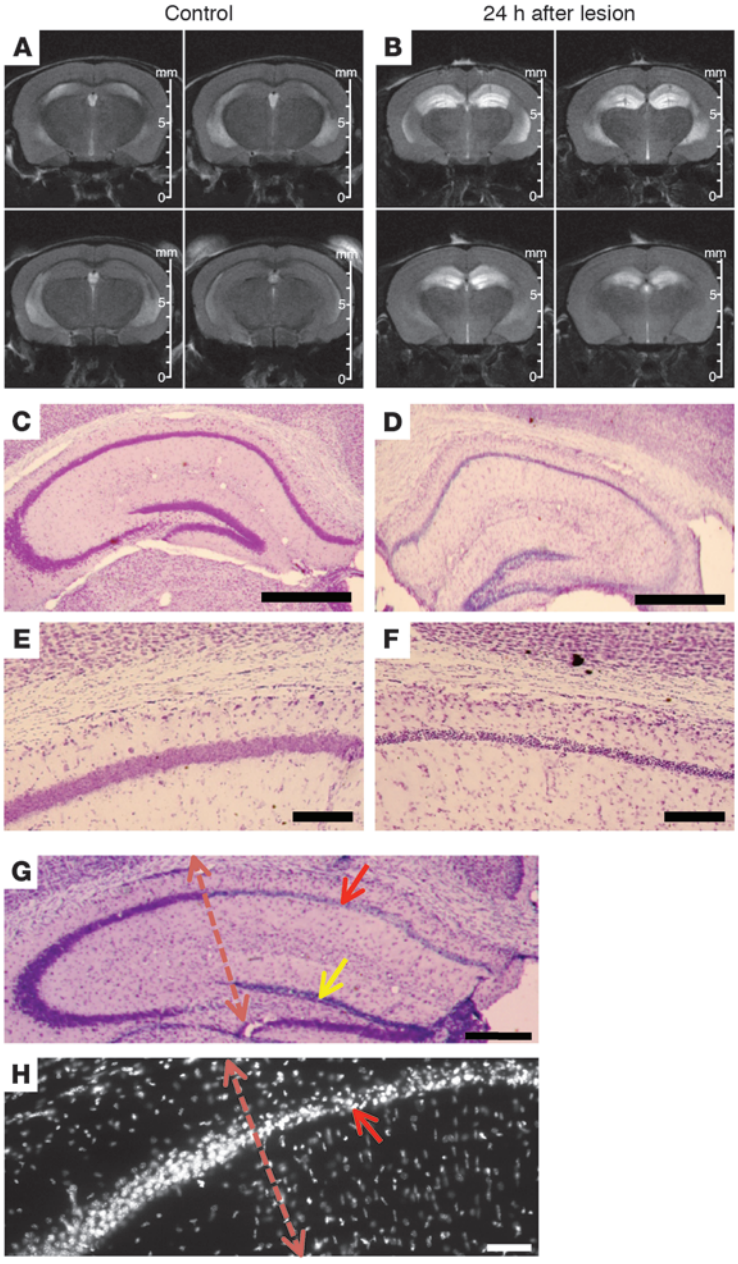

Figure 2
Lesion assessment. 24 hours after IH ibotenic acid injections, lesion extent was assessed in vivo by MRI (**A** and **B**). Examples of 4 axial contiguous T2-weighted images (slice thickness = 500 μm, TE_{eff} = 60 ms, TR = 3000 ms, rare factor = 8; 8 averages) from control (**A**) and lesioned (**B**) mice are shown. In (**B**), the hypersignal (bright intensity) revealed the extent of the injury. Extent of ibotenic acid–induced neuronal death was visualized using cresyl violet staining (**C**–**F**). When compared with controls (**C** and **E**), lesioned mice exhibited a dramatic cell loss in the whole hippocampus (**D**). High magnification images of CA1 pyramidal cell body layers in control and lesioned mouse are shown in **E** and **F**, respectively. In **G** (crystal violet staining) and **H** (Hoechst blue staining), region-specific lesions in stratum pyramidale of the CA1 (red arrow) and upper part of the stratum granulosum layer DG (yellow arrow) demonstrate their efficiency and specificity when compared with neighboring intact layers. Scale bars: 500 μm (**C** and **D**); 100 μm (**E** and **F**); 250 μm (**G** and **H**).

excluded from the study (n = 4). The extent of neurodegeneration, assessed by visualizing edema volume on each scan, was 2.5 mm (± 0.5) when the anteroposterior axis was considered. The pyramidal and granular layers (CA1-3, DG) were significantly damaged (Figure 2, C–F). To better appreciate cellular loss efficiency, we performed region-specific lesion (stratum pyramidale of the CA1 and upper part of the stratum granulosum layer DG) of a hippocampus and observed a reduction of the cell layer density when compared with neighboring intact layers (stratum pyramidale of the CA2/CA3 and lower part of the stratum granulosum layer DG) of the same hippocampus (Figure 2, G and H). Mnesic performances of each mouse were assessed 3 weeks after lesion and 4 weeks after transplantation, either in the olfactory tubing maze or the Morris water maze.

Hippocampal-dependent associative memory assessment in the olfactory tubing maze. We first used the olfactory tubing maze and an associative memory paradigm that we previously devised (29). Three weeks after the lesion was induced, water-deprived mice (n = 24) were trained to associate a banana synthetic odor with a drop of water and a lemon synthetic odor with a nonaversive sound in a dedicated maze (Supplemental Video 1; supplemental material available online with this article; doi:10.1172/JCI44489DS1). As shown in Figure 3A, lesioned mice (n = 16) were unable to learn the cue-reward associations across the 5 training sessions and responded randomly in comparison with control mice (n = 8) (multiple ANOVA [MANOVA], $F_{[1,22]}$ = 8.68, P = 0.007). Animals exhibiting correct lesions were selected for grafting of human GFP^+ OE-MSCs at the initial sites of ibotenic acid delivery (225,000 cells per hemisphere; grafted intrahippocampal [IH] group, n = 8) or culture medium (sham-grafted IH group, n = 8). Four weeks after transplantation, associative memory was retested according to the same procedure. Statistical analyses of the percentage of correct responses revealed a significant group effect (MANOVA, $F_{[2,21]}$ = 16.426; P < 0.001). The group effect was due to significantly impaired performance in lesioned mice, whether sham-grafted or grafted (IH), overall percentage of correct responses being significantly decreased in these 2 groups when compared with control mice (P < 0.001 and P = 0.037, respectively). However, as shown in Figure 3B, transplanted mice significantly improved their ability to perform correct associations when compared with sham-grafted animals (P = 0.021). Interestingly, grafted animals dramatically improved their learning capabilities across the 5 training sessions and exhibited scores close to those of control animals, while sham-grafted animals continued to respond randomly. Additionally, intertrial interval analysis revealed no significant difference between sham-grafted (28.63 s SEM ± 1.44) and grafted (IH) (28.3 s SEM ± 1.75) groups, excluding any bias related to variations in motor function. To confirm the validity of our findings, the olfactory cue–based test was backed up by a visual cue–based memory assessment using the Morris water maze.

Hippocampal-dependent reference memory assessment in the Morris water maze. To evaluate visuospatial learning and reference

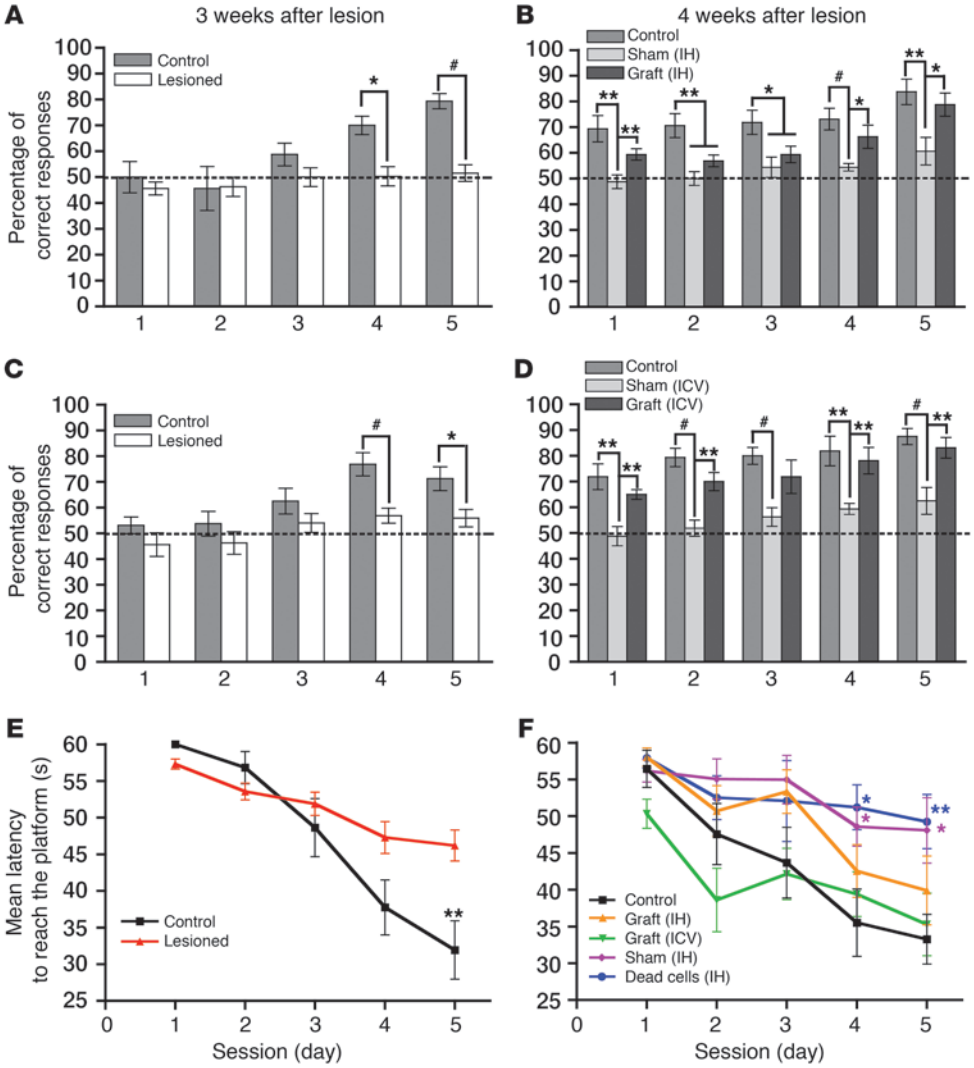

Figure 3

IH and ICV transplantation of human OE-MSCs improved hippocampus-dependent learning and memory. Cognitive capacities of mice were assessed in the olfactory tubing maze (**A**–**D**) and the Morris water maze (**E** and **F**). Associative or spatial memory in mice was assessed 3 weeks after lesion (**A**, **C**, and **E**) and 4 weeks after cell or culture medium transplantation (**B**, **D**, and **F**). (**A**–**D**) Mean percentage of correct responses was obtained during 5 training sessions of 20 trials per day. (**A** and **C**) Lesioned mice ($n = 2 \times 16$) exhibited significant impairment in an associative memory task when compared with control mice ($n = 2 \times 8$). 4 weeks after cell implantation in the lesioned sites (**B**) or in the lateral ventricles (**D**), grafted mice (grafted, $n = 2 \times 8$) demonstrated a significant improvement in associative memory when compared with vehicle-grafted mice (sham-grafted, $n = 2 \times 8$). (**E** and **F**) Graphs showing the mean latencies to reach the platform during 5 training sessions of 4 trials per day. (**E**) Lesioned mice ($n = 32$) exhibited significant impairment in a visuospatial learning task when compared with control mice ($n = 8$). 4 weeks after cell implantation in the lesioned sites (grafted IH, $n = 8$) or in the lateral ventricles (grafted ICV, $n = 8$), grafted mice demonstrated a significant improvement in spatial learning and memory when compared with vehicle-grafted mice (sham-grafted and dead cells, $n = 8$, respectively). See also Supplemental Table 1 and Supplemental Videos 1 and 2. $^{*}P < 0.05$; $^{**}P < 0.01$; $^{\#}P < 0.001$.

memory, a second series of mice ($n = 32$) were trained to find an immersed platform in the Morris water maze (ref. 30 and Supplemental Video 2). Lesions were found to induce dramatic deficits in spatial learning as shown by the significant difference in the mean escape latencies between control and lesioned groups (MANOVA, $F_{[1,38]} = 4.66$; $P = 0.037$) (Figure 3E). As shown in Figure 3E, at day 5, control mice reached the submerged platform significantly faster (31.9 s SEM ± 3.9) when compared with lesioned mice (46.2 s ± 2.1) (ANOVA, $F_{[1,38]} = 9.307$; $P = 0.004$), while no difference was observed in the swimming speed between control (11.10 cm/s ± 0.87) and lesioned mice (10.98 cm/s ± 0.36). Twenty-four hours later, probe test showed a significantly longer time spent in the platform quadrant (Q1) by control mice, whereas no difference was observed in the lesioned group (Supplemental Table 1). The latter data indicate a reference memory deficit, consecutive to the lesion. After confirming the lesion efficiency, a strictly similar protocol was applied for both grafted IH and sham-grafted IH groups. Moreover, we used an additional control group, which included mice grafted with dead OE-MSCs at the initial lesion sites (dead cells IH group, $n = 8$). Four weeks after transplantation, MANOVA of the latencies to reach the platform revealed a significant group effect ($F_{[3,28]} = 4.41$; $P = 0.012$). The group effect was due to impaired performance in sham-grafted IH ($P = 0.023$) and dead cells IH groups ($P = 0.024$): latencies were significantly increased in these 2 groups when compared with control group, whereas no significant difference was observed for the grafted IH group ($P = 0.406$) (Figure 3F). Again, we observed a positive effect of OE-MSCs grafts, as indicated by the significant decrease in the latencies to reach the platform across the 5 training sessions, when compared with both sham-grafted IH and dead cell groups. Noticeably, swimming speed analysis revealed no intergroup difference (ANOVA, $F_{[3,34]} = 2.465$; $P = 0.081$). Probe test analyses revealed a significantly longer time spent in the platform quadrant (Q4) by both control and grafted IH groups, whereas no significant difference was observed in lesioned and dead cell groups (Supplemental Table 1).

Transplantation of human OE-MSCs restores synaptic transmission and long-term synaptic plasticity

Electrophysiological recordings were performed in order to substantiate behavioral data. At the end of the cognitive tests, 20 mice

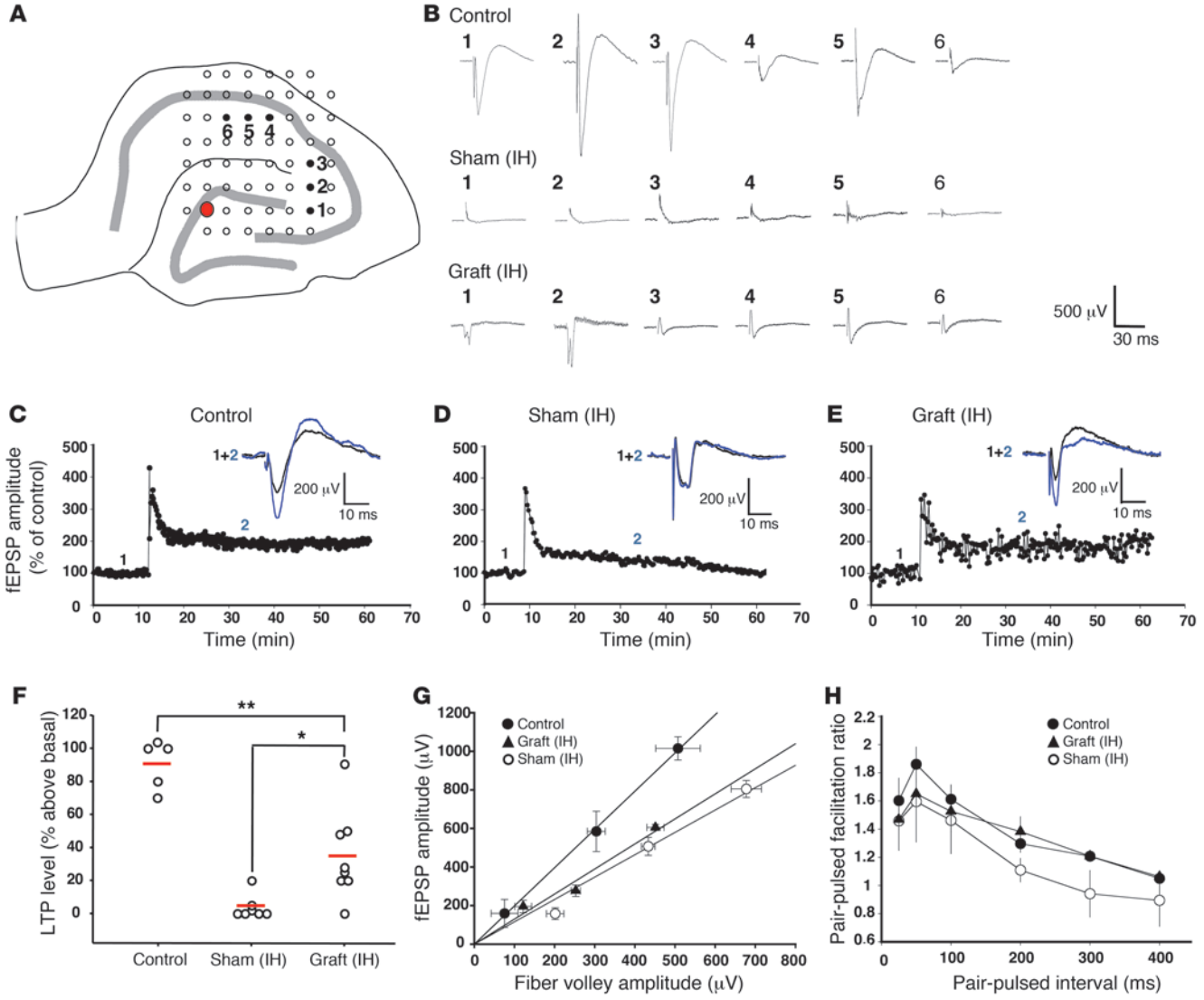

Figure 4

Recovery of excitatory synaptic transmission and LTP after human OE-MSC transplantation in lesioned hippocampi. 5 weeks after cell grafting, acute hippocampal slices were prepared and synaptic transmission was evaluated with a multi-electrode array. (**A**) Schematic diagram illustrating the positioning of hippocampal slices on a 60-electrode array. fEPSPs were evoked along the hippocampal circuitry by delivering stimulations (red electrode) in the DG. Recording electrodes (1 to 6) were located in CA1 and CA3 subfields. (**B**) Representative fEPSPs from control, sham-grafted, and grafted mice. A partial recovery of evoked fEPSPs was observed in slices from grafted but not in vehicle-treated mice. (**C**–**F**) The same setting was used to record CA1 LTP. Illustrative examples of LTP triggered by high-frequency stimulation are shown in control (**C**), sham-grafted (**D**), and grafted (**E**) mice. fEPSP amplitude was normalized against control values and plotted. (**F**) Group data for LTP in control ($n = 5$), sham-grafted ($n = 7$), and grafted ($n = 8$) mice; mean values of LTP levels (measured 40 minutes after HFS) are indicated with an horizontal bar (each animal is represented by a circle). (**G**) Basal synaptic transmission in control ($n = 4$), sham-grafted ($n = 4$), and grafted ($n = 4$) mice. The input/output curve was generated by applying increasing stimulation intensities and by plotting the fEPSP amplitude as a function of the corresponding fiber volley amplitude. (**H**) Group data for paired-pulse facilitation in control ($n = 4$), sham-grafted ($n = 4$), and grafted ($n = 4$) mice. $^*P < 0.05$; $^{**}P < 0.01$.

were sacrificed, acute hippocampal slices were prepared, and integrity of the trisynaptic hippocampal circuitry (loop DG-CA3-CA1) was tested using a multielectrode array including 60 extracellular electrodes. Electrical stimulation was delivered in the DG cell body layers and evoked responses (field excitatory postsynaptic potentials [fEPSPs]) were measured in CA3 and CA1 subfields (Figure 4A). Compared with control mice, almost no EPSP was elicited in CA3 and CA1 in slices from sham-grafted animals. In contrast, although of smaller amplitude when compared with control group, fEPSPs were recorded in CA1 following DG stimulation in slices from grafted animals (Figure 4B).

Then we investigated whether this improvement was associated with changes in LTP in the CA1 subfield, by applying a train of high-frequency stimulation (100 Hz, 1 s) to the Schaffer collateral pathway. Forty minutes after high-frequency stimulation, LTP magnitude was 90% ± 6% ($n = 5$) in control animals (Figure 4C),

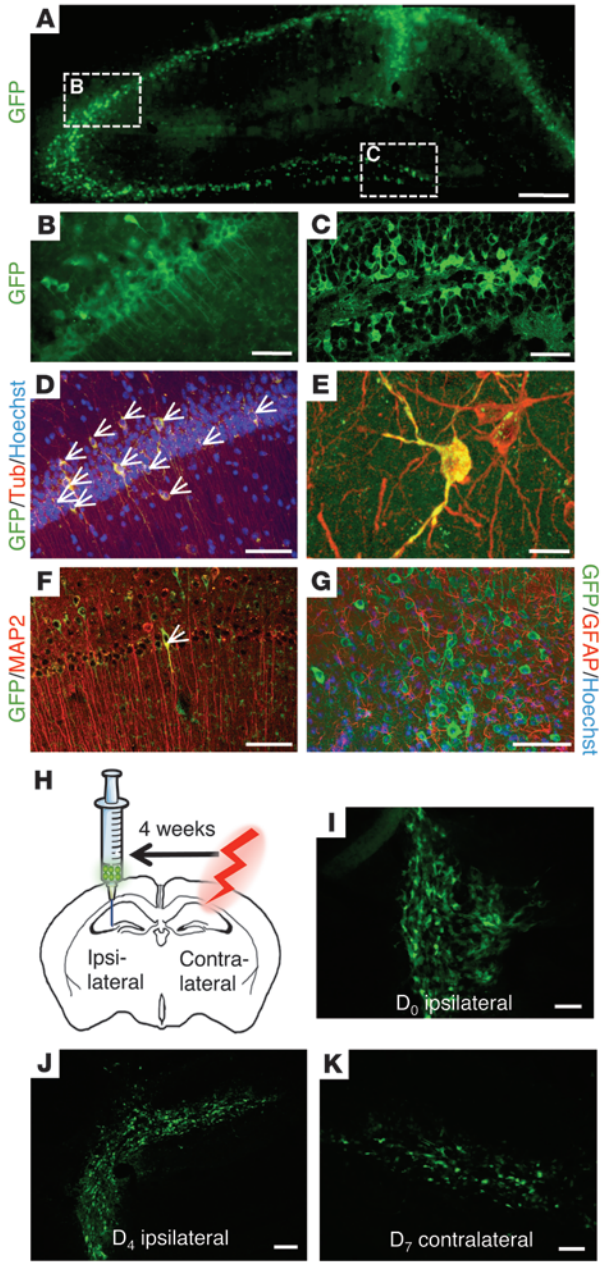

Figure 5
Human OE-MSCs transplanted into lesioned mouse hippocampi survived, migrated, and differentiated into neurons. (**A**) 5 weeks after transplantation, exogenous GFP+ human OE-MSCs were present in the different fields (CA1, CA3, DG) of the lesioned hippocampus. (**B** and **C**) GFP+ human OE-MSCs were mostly found in pyramidal (CA3, **B**) and granule cell layers (DG, **C**). (**D**) Within these layers, a high proportion (69%) of GFP+ human OE-MSCs (green) expressed III–β-tubulin (red) (white arrows in **D**). (**E**) High magnification of the merged picture of human GFP+ OE-MSCs (green) expressing III–β-tubulin (red). (**F**) A small proportion of human GFP+ OE-MSCs (green) expressed MAP2 (white arrow), a marker for mature neurons (red). (**G**) No GFP+ human OE-MSC (green) was ever found to express the astrocytic marker GFAP (red). (**H**) 4 weeks after lesioning the right hippocampus, GFP+ OE-MSCs were transplanted into the intact hippocampus (i.e., left hemisphere). At day 0 (D_0) after transplantation, cells formed clusters and were only observed within the injection site as a cell cluster (**I**). At D_4 after transplantation, numerous GFP+ cells were observed migrating outside the injection site toward the contralateral lesioned hippocampus (**J**). At D_7 after transplantation, few GFP+ OE-MSCs were observed inside the contralateral hippocampus (**K**). Scale bars: 250 μm (**A**); 200 μm (**J**); 100 μm (**B**, **C**, **D**, **F**, **G**, **I**, and **K**); 20 μm (**E**). See also Supplemental Video 3.

while it was almost completely abolished in sham-grafted animals (4% ± 9%, $n = 7$) (t test; $P < 0.001$) when signals could be recorded in the CA1 area (Figure 4D). In contrast, a significant recovery of LTP (35% ± 10%, $n = 8$) was observed in grafted animals when compared with sham-grafted (t test; $P = 0.0119$) (Figure 4, E and F). However, LTP in grafted animals remained significantly lower when compared with LTP recorded in control animals (Figure 4F) (t test; $P = 0.0019$). Additionally, EPSPs zeroed after perfusion of NBQX, an AMPA receptor antagonist, confirming the synaptic nature of recorded EPSPs (data not shown).

In parallel, we investigated whether lesioning and cell grafting altered basal synaptic transmission and short-term synaptic plasticity. Basal synaptic transmission was studied by generating the input/output curve. The fEPSP amplitude obtained at various stimulus intensities was plotted against the corresponding fiber volley amplitude (Figure 4G). In control animals, we observed a linear relationship with a slope value of 1.92 ($n = 4$; $r^2 = 0.91$). Lesioning the animals led to a change in the synaptic signals, as the slope of the curve was flattened to 1.20 ($n = 4$; $r^2 = 0.94$). In grafted animals, the slope was 1.13 ($n = 4$; $r^2 = 0.71$), not significantly different from values obtained in sham-grafted animals. Short-term synaptic plasticity was evaluated by pairing stimuli at intervals ranging from 25 to 400 ms. No significant change was detected in sham-grafted and grafted animals when compared with control group, although in lesioned animals, there was a lower paired-pulse ratio for the interstimulus intervals of 200, 300, and 400 ms (Figure 4H).

Human OE-MSCs survive, migrate, differentiate into neurons, and stimulate endogenous neurogenesis in mouse lesioned hippocampus

The functional recovery following transplantation was associated with an exogenous neurogenesis. Five weeks after transplantation, we found that 60,000 to 90,000 exogenous cells (survival rate ranging from 13% to 20%) had settled within the hippocampus. A large proportion of GFP+ cells were distributed along the different damaged hippocampal fields, including CA1, CA3, and DG (Figure 5, A–C). While 69% ± 11% of the OE-MSCs were expressing III–β-tubulin, an immature neuron marker, and 0.9% ± 0.4% were positive for MAP2, a mature neuron marker (Figure 5, D–F), none of the exogenous cells were immune-positive for the astrocytic marker GFAP (Figure 5G). Moreover, GFP+ cells were also observed in other cerebral areas, especially in cortices above the hippocampus (Supplemental Video 3). Not a single exogenous cell was found in peripheral structures such as kidneys, liver, or lung (data not shown). An additional experiment, based on transplantation of human OE-MSCs in unilaterally unlesioned hippocampus, demonstrated that stem cells migrated toward the contralateral lesioned hippocampus (Figure 5, H–K). Interestingly, transplantation of OE-MSCs in bilaterally unlesioned hippocampi showed that cells do not migrate and stay within the tract generated by the injecting needle.

To quantify the impact of human OE-MSCs on endogenous hippocampal neurogenesis, newborn cells were labeled with the thymidine analog BrdU. In each group ($n = 5$ per group), the per-

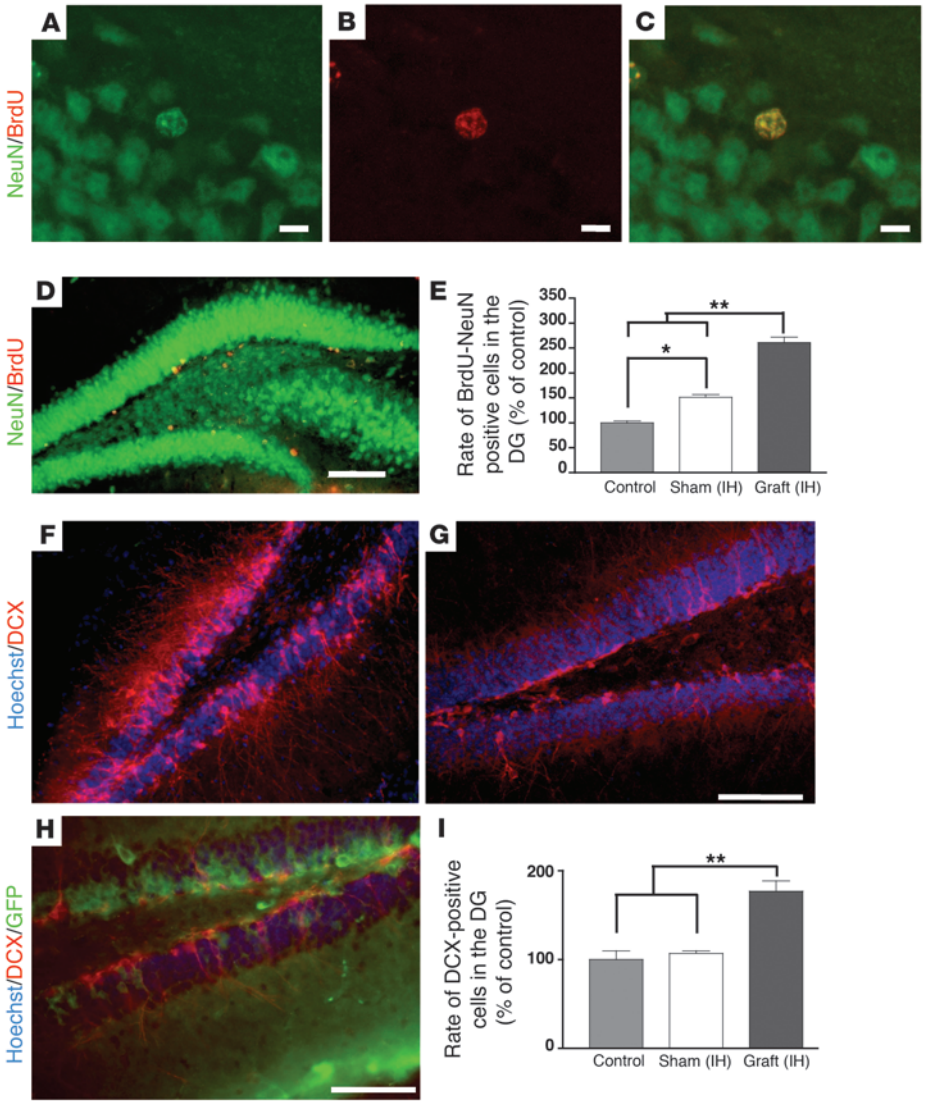

Figure 6
Human OE-MSCs stimulated endogenous neurogenesis after transplantation in lesioned hippocampi. 5 weeks after grafting, brain sections of mice injected with BrdU twice a day during 3 days following cell implantation (n = 5 for each group) were immunostained with anti-NeuN (green) and anti-BrdU antibodies (red) (**A**–**D**). Quantification of BrdU$^+$/NeuN$^+$ cells in DG indicated an increased number of mitotic cells in grafted (IH) mice when compared with sham-grafted (IH) ($P < 0.05$) and control ($P < 0.01$) mice (**E**). DCX immunohistochemistry revealed the presence of immature neurons in the DG of control (**G**) and grafted (IH) (**F**, **H**) mice. As shown in (**H**), no GFP$^+$ human OE-MSC was found to express DCX. Lesioned mice with IH transplant of human OE-MSCs (grafted [IH], n = 5) exhibited a higher percentage of DCX-positive cells when compared with vehicle-treated (sham-grafted [IH], n = 5) and control (n = 5) mice (**I**). (**E** and **I**). Scale bars: 10 μm (**A**–**C**); 100 μm (**D**, **F**, **G**, and **H**). *$P < 0.05$; **$P < 0.01$.

centage of newly formed neurons expressing BrdU and NeuN was determined 5 weeks after the last BrdU injection (Figure 6, A–E). No GFP$^+$ cell was found to be BrdU positive and no tumor formation was ever observed. In confirmation, we found that not a single exogenous cell was positive for Ki67 (data not shown). Moreover, we performed a comparative CFSE proliferation assay showing that, in our culture conditions and prior transplantation, sphere-derived cells are not proliferative or are poorly proliferative (Supplemental Figure 1). Additionally, we quantified a significant increased neurogenesis within the subgranular zone and granule cell layers of the DG in both sham-grafted (P = 0.032) and grafted groups (P = 0.008) when compared with control group. The number of BrdU$^+$/NeuN$^+$ cells was approximately 1.5-fold and 2.5-fold higher in the sham-grafted group and in the grafted group, respectively. Moreover, newly generated neurons were significantly more numerous in the grafted group when compared with the sham-grafted group (P = 0.008). We also labeled immature neuronal cells with doublecortin (DCX) antibody, in order to assess the state of the endogenous neurogenesis just before sacrifice, 5 weeks after transplantation (Figure 6, F–H). Surprisingly, no GFP$^+$ exogenous cell was found to be DCX positive (Figure 6H). We observed a 1.8-fold increase in the number of endogenous DCX-positive cells in the grafted group when compared with either sham-grafted or control groups ($P < 0.01$) (Figure 6I).

Human OE-MSCs grafted within the lateral ventricles, survive, migrate, differentiate, and restore mnesic capacities

The positive results obtained during this first series of experiments led us to modify 1 of our 3 initial options. Using the same animal model, we decided to graft GFP$^+$ OE-MSCs, derived from a single stem cell, within the cerebrospinal fluid of lateral ventricles. As previously described, we first confirmed the lesion efficiency in both tests (Figure 3, C and E). Four weeks after transplantation, behavioral assessment using the olfactory tubing maze revealed a significant group effect (MANOVA, $F_{[2,21]} = 34.839$; $P < 0.001$). The group effect was due to significantly impaired performance in lesioned mice (sham-grafted intracerebroventricular [ICV] group), with an overall percentage of correct responses significantly decreased in this group when compared with control ($P < 0.001$) and grafted ICV groups ($P < 0.001$). Across the 5 train-

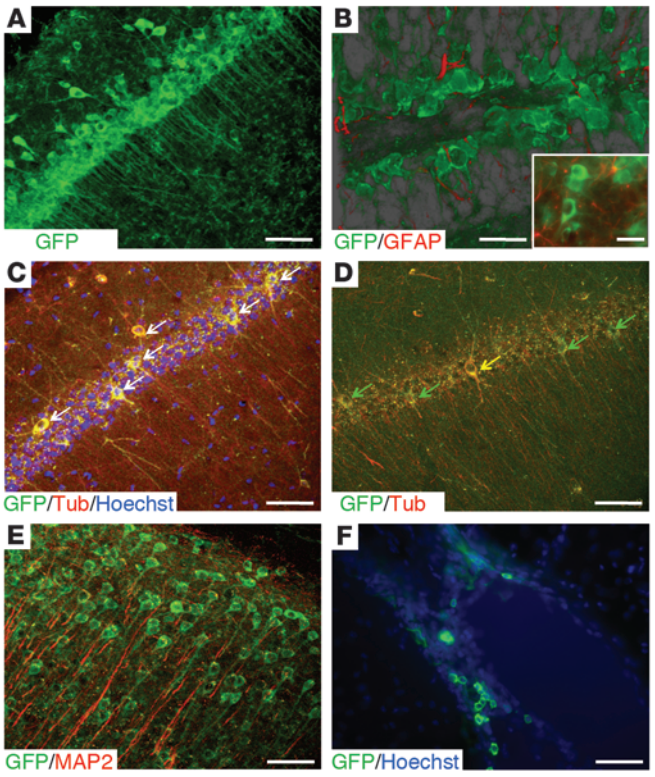

Figure 7
Human OE-MSCs transplanted into the cerebrospinal fluid (CSF) of hippocampus-lesioned mice survived at least 5 weeks, migrated, and differentiated into neurons. (**A**) Increased density of GFP$^+$ cells within the pyramidal cell body layers demonstrated the ability of human OE-MSCs to migrate from the CSF toward the injury zone. (**B**) As demonstrated by confocal image reconstitution using projection transparency (see also Supplemental Video 4), exogenous GFP$^+$ cells were also remarkably distributed within the granule cell body layers of the DG. The insert indicates that not a single human OE-MSC expressed the astrocytic marker GFAP (red). (**C** and **D**) Within the CA3 field, some pyramidal cell–like and interneuron-like GFP$^+$ human OE-MSCs (green) expressed III–β-tubulin (red) (white arrows in **C**, yellow arrow in **D**), but others were immunonegative for this immature neuronal marker (green arrows in **D**). (**E**) Exogenous GFP$^+$ cells migrated as well in other cerebral areas (cortical area in **E**), but remained immunonegative for the mature neuronal marker MAP2 (red). (**F**) GFP$^+$ cells exhibiting an undifferentiated morphology were found at the margin of the ventricular areas. Scale bars: 100 μm (**A**, **C**, **D**, **E**, and **F**); 30 μm (**B**, insert). See also Supplemental Video 4.

ing sessions, grafted animals improved their mnesic capacities significantly, while sham-grafted animals remained unable to perform the task (Figure 3D). Intertrial interval analysis revealed no significant difference between sham-grafted (31.12 s SEM ± 2.16) and grafted (ICV) (28.42 s SEM ± 1.7) groups. In parallel, analysis of latencies in the Morris water maze test revealed a significant group effect ($F_{[3,28]} = 10.473$; $P < 0.001$). The group effect was due to significantly impaired performance in sham-grafted ($P = 0.009$) and dead cell groups ($P = 0.009$), with latencies significantly increased in these 2 groups, when compared with control and grafted ICV groups. No significant difference was observed between grafted ICV and control groups ($P = 1$) (Figure 3F). Whereas no significant difference was observed in the swimming speed between grafted ICV and both sham-grafted ($P = 0.1$) and control ($P = 1$) groups, similar analysis revealed that grafted mice with dead cells were significantly faster when compared with those in the grafted ICV group ($P = 0.01$). Probe test analyses revealed a significantly longer time spent in the platform quadrant (Q4) by both control and grafted ICV groups, while no significant difference was observed in lesioned and dead cell groups (Supplemental Table 1).

Improved mnesic performances were also associated with the presence of GFP$^+$ cells in the different layers of the lesioned hippocampi (Figure 7, A and B, and Supplemental Video 4). An extensive exogenous neurogenesis was observed, with stem cells differentiating into cells expressing neuron-specific markers (Figure 7, C and D). No GFP$^+$/GFAP$^+$ cell was ever encountered. Exogenous cells were found in cortical areas but remained always immunonegative for the mature neuronal marker MAP2 (Figure 7E), and no GFP$^+$ cell was found in peripheral structures. Conversely, GFP$^+$ cells exhibiting an undifferentiated morphology and negative for neural markers (III–β-tubulin, MAP2, GFAP) were found at the margin of ventricular areas (Figure 7F). Regarding these data, we expected a migratory potential of OE-MSCs in response to specific signals generated by a lesion.

Lesioned hippocampi overexpress genes involved in cell chemoattraction

In order to understand OE-MSC homing, a comparative gene expression profile of lesioned and control hippocampi (3 vs. 3) was performed using mouse pangenomic DNA microarrays 4 weeks after surgery. In total, 114 transcripts with a fold change above 2.5 were found upregulated in lesioned hippocampi. The list of overexpressed genes indicates that 53% were involved in immune and inflammatory processes, 22% in cell metabolism, and 27% in various other processes (Supplemental Figure 2). Interestingly, among overexpressed genes, 8% code for chemokines and 2 of them, *Ccl2* and *Cxcl10*, have a fold change above 10 (Table 1). Moreover, cytokines such as *Spp1* and *C3*, known for their chemotactic properties, were also upregulated with a fold change of 11 and 162.5, respectively.

Discussion

Stem cells are present in most adult tissues, where they contribute to tissue regeneration. Such a feature is also observed in the olfactory mucosa, which has an extraordinary capacity to functionally self regenerate. Until recently, basal stem cells (horizontal and globose), located in the olfactory epithelium, were identified as the only 2 stem cells types in the nasal cavity (31). However, a new olfactory stem cell subtype, previously suspected to reside inside the lamina propria (15), has been confirmed and characterized by 2 distinctive groups at the same time (16, 17). Although the biological function of these ectomesenchymal stem cells remains to be unveiled, our present study and previous data suggest that these cells could be useful for stem cell therapies (15, 32, 33). We report here what we believe is the first successful restoration of learning and memory after transplantation of adult human olfactory nasal stem cells, derived from the lamina propria, in a murine model that mimics effects of ischemic/hypoxic injury in the hippocampus exclusively (28). As a result, it is possible that this new stem cell type can be used for repairing the damaged or pathological brain.

Table 1
Dysregulated transcripts coding for chemokines with a fold change above 2.5 in lesioned hippocampus in comparison with control

Gene symbol	Gene name	Fold change
Ccl2/Mcp1	Chemokine (C-C motif) ligand 2 Monocyte chemoattractant protein 1	24.2
Cxcl10/Ip-10	Chemokine (C-X-C motif) ligand 10 Interferon-inducible cytokine IP-10	11.7
Ccl19/Mip3b	Chemokine (C-C motif) ligand 19 Macrophage inflammatory protein 3b	4.8
Ccl4/Mip1b	Chemokine (C-C motif) ligand 4 Macrophage inflammatory protein 3b	4.7
Ccl5	Chemokine (C-C motif) ligand 5/RANTES	4.7
Cxcl16	Chemokine (C-X-C motif) ligand 16	3.7
Ccl7/Mcp3	C-C motif chemokine 7 Monocyte chemoattractant protein 3	3.2
Ccl12/Mcp5	C-C motif chemokine 12 Monocyte chemoattractant protein 5	2.9
Cxcl1/Gro1	C-X-C motif chemokine 1 Growth-regulated α protein	2.6 2.6

See also Supplemental Figure 1.

Although no immunosuppressant was delivered to the host animal, we found that a relatively large fraction (nearly 20%) of injected human cells invaded the hippocampal neuronal layers and that the vast majority (nearly 70%) differentiated into cells expressing neuronal markers (III–β-tubulin, MAP2) and not glial marker (GFAP). In contrast to what has been observed in other transplantation studies (6, 34) and despite our previous experiments demonstrating that olfactory mucosa spheres can be driven to generate astrocytes and/or neurons under defined conditions in vitro (15), none of the grafted cells differentiated into astrocytes. Similarly, in our in vitro coculture experiment, no OE-MSC–derived astrocyte was ever observed. These surprising findings may be due to our initial choice of exclusively lesioning the hippocampus. A previous in vitro study demonstrated that factors from this neurogenic brain area induced the differentiation of mesenchymal stem cells into neurons exclusively, and stem cell–derived astrocytes were found only when soluble factors were collected from the cortex or the cerebellum (27). Conversely, it has been shown by others that SVZ neural stem cells, dedicated to producing dopaminergic or GABAergic neurons, differentiate only into glial lineages when transplanted ectopically (35). Accordingly, our data confirm the importance of the microenvironment in the differentiation process. It remains now to be seen whether similar outcomes can be achieved when olfactory stem cells are implanted in another lesioned cerebral area.

The central nervous system is known for being at least partially immunoprivileged (36), and we took advantage of this specificity to perform xenotransplantations without the use of any immunosuppressant. Moreover, it has been demonstrated that mesenchymal stem cells display specific immune properties including hypoimmunogenicity and immunoregulatory and immunosuppressive activities (37). As a result, human mesenchymal stem cells are not fully rejected by the CNS of rodent recipients.

When compared with BM-MSCs, OE-MSCs in vitro exhibit a high proliferating profile under defined conditions and can be grown in large numbers. Here we show that specific culture conditions for sphere formation inhibit cell proliferation. This could explain why not a single dividing human cell has been found after brain implantation, as observed by BrdU and Ki67 staining. This result indicates that, unlike embryonic stem cells (10), sphere-derived OE-MSCs are not prone to proliferation after brain transplantation. This property is obviously valuable and might be considered to represent a prerequisite for clinical trials based on cell therapy. In addition, as previously described in studies using mesenchymal and neural stem cell types (38), postmitotic OE-MSCs were able to boost the proliferation of resident stem cells. To date, the mechanisms by which OE-MSCs trigger endogenous neurogenesis remain largely unknown. However, in a parallel in vitro study, we found that OE-MSCs release trophic factors, triggering a significant increase in neurite length (data not shown). Together, these data support the hypothesis that OE-MSC transplantation creates a permissive microenvironment that stimulates endogenous neurogenesis and helps to restructure preexisting networks acting on resident neural stem cells and neurons.

Although temporally simultaneous, the dual process of endogenous neurogenesis and exogenous neuronal differentiation exhibit dissimilarities. Resident stem cells proliferate and give rise to functional neural stem cells (39) but display a limited migration. In contrast, exogenous stem cells stop multiplying and differentiate into neurons after a protracted migration to the damaged neuronal layers. We recently showed that OE-MSCs can be considered as a mesenchymal stem cell subtype with neurogenic properties (17). It is well established that mesenchymal stem cells are able to cross physical and metabolic frontiers such as the blood-brain barrier. Moreover, analysis of gene overexpression in lesioned hippocampus provides molecular signature evidence for the site-specific migration process observed in this study. This site-specific attraction could be similar to leukocyte trafficking and occurs via inflammation-associated factors, such as chemotactic cytokines or chemokines (40). Here, we demonstrate that many inflammatory molecules are still expressed in lesioned hippocampi 4 weeks after lesioning. We observed a robust overexpression of 9 genes coding for chemokines that could provide a chemoattractant microenvironment supporting the migration of OE-MSCs. *Ccl2* (*Mcp-1*), the most overexpressed chemokine in lesioned hippocampus, is known to have chemoattractive properties on mesenchymal stem cells (41) or neural stem cells (42, 43). Similarly, *Cxcl10*, another overexpressed chemokine, stimulates migration of mesenchymal stem cells (44). Two other strongly overexpressed genes coding for cytokines with chemoattractive properties, *C3* and *Spp1*, could be involved in the OE-MSC–directed migration. SPP1 (osteopontin) exerts a chemoattractive effect on stem cells by recruiting mesenchymal stem cells via CD44 (45) or regulating the migration of neuroblasts to injured cerebral structures (46). The protein encoded by *C3*, via the formation of C3a, also plays a chemoattractive role for mesenchymal stem cells (47). In addition, we observed that OE-MSCs express several chemokine receptors and are responsive to overexpressed molecules that stimulate their migration (data not shown). It is therefore not surprising that OE-MSCs can home to lesioned sites, and this selective migration is a critical step in stem cell regenerative therapies.

The significant neurogenic effects observed in these experiments were associated with partial recovery of LTP and a remarkable

recovery of learning and memory abilities. Surprisingly, such findings are correlated with the reestablishment of neuron networks mostly displaying the immature marker III–β-tubulin. However, previous studies reported that immature neurons express a more robust LTP than mature neurons (48, 49), supporting the hypothesis that immature neurons derived from a pool of endogenous stem cells (50) and/or exogenous stem cells in our study could contribute to the formation of a new mnesic trace. Combined with our data showing that OE-MSCs induce neuronal maturation/stimulation via trophic factors, it can thus be envisaged that exogenous cells participate in the reestablishment of a functional network. Otherwise, it has already been shown that embryonic (51) or neural (52) stem cells can form functional synapses and integrate into the host cortical circuitry after transplantation into the developing brain. Although previous studies have demonstrated hippocampal plasticity after cell transplantation (53–56), to the best of our knowledge, no study using human adult stem cells has ever demonstrated that cell therapy can induce the restoration of functional neuronal networks within the adult hippocampus. Grafting neural stem cells, sampled from the brain, was previously shown to improve learning capacities of lesioned adult mice (6). While these results suggest that both types of stem cells could potentially be used for future treatments of memory loss, nasal olfactory stem cells present numerous advantages for a medical application.

Indeed, among all the cell types proposed for the future regenerative medicine of the CNS, OE-MSCs have the enormous advantage of being easily accessible in living adults, obtainable under local anesthesia, and transplantable in an autologous manner, thus eliminating contentious ethical and technical considerations (57). By overcoming these 2 major hurdles, the use of OE-MSCs in clinical trials protocols should be facilitated, representing a first step for the translation to the clinic. In addition, the proof of principle that olfactory ensheathing cells, also derived from the nasal lamina propria, can be safely used in clinical protocols for spinal cord injury has been recently established. Moreover, and contrary to other cell types like BM-MSCs, nasal stem cells already reside in a neural environment, which represents a nonnegligible benefit for targeting brain disorders. Considering that the time window after injury is a critical point for using cell therapy, the short time scale necessary for the isolation and expansion of OE-MSCs is important to consider. As a consequence of their highly proliferative capacity in vitro under the control of defined factors, the number of cells is not a limiting factor.

Methods

Experimental design

We performed the ibotenate lesion on experimental day 1 followed by a control of the lesion efficiency, using MRI, at day 2. A functional control, using behavioral tests, was performed at week 3. Human OE-MSCs were transplanted at week 4, and animals were retested at week 8 before being sacrificed for either electrophysiological or immunohistological analyses. Anesthesia and surgical procedures were performed according to the French law on Animal Care Guidelines, and the Animal Care Committee of Aix-Marseille University approved our protocols. Human biopsies were obtained under a protocol that was approved by the local ethical committee (Comité de Protection des Personnes) of Marseille. Informed consent was given by each individual participating in the study, in accordance with the 1964 Helsinki convention and French law relating to biomedical research.

Animals

Adult male Balb/c mice (n = 77) and C57BL/6 (n = 40) (IFFA CREDO), 10 weeks old at the beginning of the experiment, were used. All animals were housed in individual cages and maintained on a 12-hour light/12-hour dark cycle at a constant temperature (22 ± 1°C). Food and water were provided ad libitum except during the habituation and training periods in the olfactory tubing maze.

Experimental injury model: amnesic syndrome

We performed a bilateral lesion of the hippocampus in mice, by using an NMDA agonist (i.e., ibotenic acid; Sigma-Aldrich) leading to the loss of neuronal cells in the sites of injection by cellular excitotoxicity. Anesthetized Balb/c (n = 46) or C57BL/6 mice (n = 32) were inserted in a stereotactic frame, the skull surface was exposed, and holes were drilled at the appropriate sites to allow bilateral infusion of ibotenic acid (10 μg/μl) with a glass capillary (40-μm external tip) glued to a 1-μl Hamilton syringe connected to stereotactic syringe pump (KDS 310; KD scientific). Antero-posterior (AP), lateral (L), and vertical (V) coordinates for micro-infusions in the hippocampus, were taken relative to the bregma: (a) AP – 1.7 mm, L ± 1 mm, V – 1.5 mm; (b) AP – 2 mm, L ± 1.3 mm, V – 1.5 mm; (c) AP – 2.6 mm, L ± 1.5 mm, V – 1.5 mm. The infused volume of ibotenic acid or PBS was 30 nl per injection site. For migration kinetic experiments (n = 4), unilateral lesions were performed (right or left hemisphere, n = 2 + 2).

MRI

Mice were anesthetized using a mixture of air and isoflurane (3% during induction and 2% for maintenance) via the nose cone of a mouse headholder device at a flow of 2 l/min. During data acquisition, body temperature was maintained at 37°C using a heating blanket. All experiments were performed with a Bruker PharmaScan spectrometer (7 T magnet and 16-cm horizontal bore size). A dedicated mouse head coil (linear birdcage coil with 23-mm inner diameter) was used for signal transmission and reception.

Sixteen axial contiguous T2-weighted images (slice thickness = 0.5 mm) with fat suppression (band width = 900 Hz) were acquired 1 day after lesion with a turbo-RARE sequence (effective echo time [TE_{eff}] = 60 ms, repetition time [TR] = 3000 ms, rare factor = 8, 8 averages), using a 21-mm field of view and 256 × 256 matrix. Mouse respiration was monitored and, to minimize motion artifacts, image acquisition was synchronized with the respiratory cycle.

Isolation and expansion of human olfactory mucosa cells

Human nasal olfactory mucosae were obtained by biopsy during routine nasal surgery under general anesthesia. Biopsies were immediately placed in growth medium containing DMEM/Ham F12 supplemented with 10% FBS and 1% penicillin/streptomycin (Invitrogen). OE-MSCs were purified from the lamina propria and cultivated as described before (17).

Generation of GFP$^+$ clonal sphere-derived OE-MSCs for transplantation

Human OE-MSCs were infected with a GFP-lentiviral vector, and sphere formation was induced as previously described (17). Individual primary spheres were dissociated and clonally replated using the limit dilution method. On the day of transplantation, floating spheres were harvested, washed, and enzymatically (trypsin/EDTA) dissociated. Sphere-derived cells were centrifuged and resuspended in serum-free DMEM-F12 at the respective concentrations of 75,000 cells/μl and 225,000 cells/μl for IH and ICV injections.

Coculture experiment

Interface hippocampal slice cultures were prepared as described previously (58). In brief, mouse hippocampal slices (250 μm) were obtained from

21-day-old Balb/c mice and plated on culture inserts. Immediately after, a drop (1 μl) of freshly prepared cell suspension (10,000 cells/μl) was laid on top of the slice. Hippocampal slices were then cultured for 21 days at 37°C, 5% CO_2, and medium was replaced 3 times per week.

Transplantation surgery

Thirty days after lesioning, mice with confirmed MRI and severe learning deficits were blindly allocated to 4 groups. In the transplanted groups (grafted groups), mice received bilateral infusions of sphere-derived human OE-MSCs (450,000 cells in total), while in the untransplanted groups, animals received an equal amount of culture medium without cells (sham-grafted groups) or dead OE-MSCs killed by 1 hour freezing step (dead cell groups). Cell suspensions or vehicle were injected with a 1 μl Hamilton syringe into the hippocampus (grafted [IH], $n = 21$; sham-grafted [IH], $n = 21$; dead cells, $n = 8$) at the same coordinates as those used for ibotenate lesion or in the lateral ventricles (coordinates: AP – 0.58; L ± 1, V – 2.1) (grafted [ICV], $n = 16$; sham-grafted [ICV], $n = 16$). The infused volume was 1 μl per injection site; the rate of infusion was 0.5 μl/min.

Behavioral procedure

The procedures using the olfactory tubing maze (29) and Morris water maze (30) have been previously described (see Supplemental Data for a full description).

Electrophysiological analyses

Experiments were carried out on acute hippocampal slices (350 μm) obtained from mice of each of 3 groups (control $n = 5$, grafted [IH] $n = 8$, and sham-grafted [IH] $n = 7$). Immediately after decapitation, brains were quickly dissected and placed in ice-cold buffer including 124 mM NaCl, 3.5 mM KCl, 25 mM $NaHCO_3$, 1.25 mM NaH_2PO_4, 1 mM $CaCl_2$, 2 mM $MgSO_4$, and 10 mM glucose (bubbled with O_2/CO_2:95%/5%). Slices were then prepared with a vibratome (VT1000S; Leica) and maintained at room temperature in the same buffer supplemented with 1 mM $CaCl_2$. Slices were transferred within the same buffer to a multi-electrode array (MEA-60; Multi Channel Systems) comprising 60 extracellular electrodes (S4). Slices were continually superfused with the medium at a flow rate of 2 ml/min^{-1} and maintained at 37°C. Monopolar stimulation was achieved with an external stimulator (MC Stimulus; Multi Channel Systems) by applying biphasic current pulses to 1 electrode of the array. Field EPSPs were then simultaneously recorded by the remaining electrodes in the dendritic subfields of hippocampal neurons. Basal synaptic transmission was monitored by delivering a 0.066 Hz stimulation. The input/output curve was generated by applying increasing stimulation intensities and by plotting the fEPSP amplitude as a function of the corresponding fiber volley amplitude. LTP was elicited by applying a 100-Hz stimulation train for 1 second. NBQX (10 μM), an AMPA receptor antagonist, was applied at the end of some experiments in order to verify that the signals recorded were effectively fEPSPs. Field EPSPs were further analyzed (MC Rack; Multi Channel Systems).

Cell quantification

The survival rate of OE-MSCs after transplantation and the percentage of transplanted OE-MSCs that expressed cell-specific marker were quantified through fluorescent microscopy. Brains were perfused and coronal sections (35 μm thick) were serially collected. The number of OE-MSCs that survived inside the hippocampus 4 weeks after transplantation was estimated by counting the number of GFP^+ cells in all sections containing hippocampus ($n = 4$ animals analyzed). The percentage of OE-MSCs that expressed cell-specific markers was estimated by counting the number of costained cells (GFP^+ + marker X) and dividing this number by the total number of GFP^+ cells in the same section. For each animal ($n = 4$), the rostrocaudal hippocampus was serially sectioned at a thickness of 35 μm, and each marker was analyzed every sixth section.

Assessment of endogenous neurogenesis

BrdU (Sigma-Aldrich) at a concentration of 6 mg/ml was injected intraperitoneally (100 mg/kg) immediately after transplantation surgery and twice a day for the next 3 days, with a delay of 8 hours between each injection. Four weeks after the last injection, brain tissues (control, sham-grafted, grafted; $n = 5$ per group) were processed (see Supplemental Experimental Procedures). Note that no behavioral assessment was performed with these mice.

Comparative quantification of $BrdU^+/NeuN^+$ cells. Comparative analysis between each group was conducted in a blind manner. Fluorescent staining of coded slides was visualized and quantified with a fluorescent microscope at ×40 and ×63. For each group, similar sections were stained and the number of $BrdU^+/NeuN^+$ cells was quantified in the subregions of the hippocampal DG, including granule cell body layer and subgranular zone. For each mouse, $BrdU^+/NeuN^+$ cell numbers were counted in 9 coronal sections (35-μm thick) covering the left DG in its rostrocaudal extension (3 dorsal sections, 175 μm apart, and 6 ventral sections, 175 μm apart), using an image analyzer (LUCIA; Laboratory Imaging). The number of $BrdU^+/NeuN^+$ cells in the control group was used as a baseline (index = 100) to evaluate changes in neurogenesis in other groups.

Comparative quantification of DCX^+ cells. Using the method described above, the number of DCX^+ cells was quantified in the granular cell body layer of the DG.

Immunostaining

Floating sections were incubated for 1 hour at room temperature (RT) with blocking buffer (3% BSA, 5% appropriate serum, 0.1% Triton X-100 in PBS) and for 90 minutes with the following primary antibodies diluted in blocking solution: rabbit polyclonal anti-DCX (1/500; Abcam), rabbit polyclonal anti-GFAP (1/500; Dako), mouse monoclonal anti–III–β-tubulin (1/500; Sigma-Aldrich), rabbit polyclonal anti-MAP2 (1/500; Chemicon), fluorescently labeled mouse monoclonal anti-NeuN (1/1000; Chemicon), rabbit polyclonal anti-GFP (1/300; Chemicon), mouse anti-GFP (1/500; Roche), monoclonal anti-BrdU (1/100; Dako), and rabbit polyclonal anti-Ki67 (1/100; Abcam). Then slices were rinsed (3 × 5 min) in PBS and incubated for 90 minutes with cross-adsorbed Alexa Fluor 488– or 594–conjugated anti-rabbit or anti-mouse secondary antibodies (1/500; Jackson Immunoresearch) in dark conditions. After several washes in PBS, slices were counterstained with 0.5 μg/ml Hoechst blue (33258; Molecular Probes) for 30 minutes and mounted with anti-fading medium (DAKO). For BrdU staining, DNA was denatured using a pretreatment in HCl [2N] and 0.2% Triton X-100 for 40 minutes at 37°C. Positive and negative controls were performed for all immunostaining of this study.

Microarray experiments

Briefly, for the Agilent microarray analysis, total RNA from freshly dissected hippocampi (3 control vs. 3 lesioned mice) were isolated 4 weeks after lesioning and then treated as described in Supplemental Methods. Genes with a fold change above 2.5 were clustered into functional groups using DAVID Functional Annotation Clustering Tool. Data are available on the ArrayExpress database (accession number E-MEXP-2682).

Statistics

All data are presented as means ± SEM. All behavioral data were analyzed by selected ANOVAs or multiple analyses of variance (MANOVAs) followed,

when appropriate, by 2 × 2 comparisons based on the Bonferroni post-hoc, using the SPSS/PC + statistics 11.0 software (SPSS Inc.). For electrophysiological and endogenous neurogenesis data, statistical significance was assessed using unpaired Student's *t* test and 2-tailed Mann-Whitney *U* test, respectively. The threshold for significance was set at $P < 0.05$.

Acknowledgments

We thank M. Baudry and I. Sancho-Martinez for comments during the preparation of this manuscript, Pierre Giraud and Laure Fronzaroli-Molinieres (INSERM U641) for their help with hippocampal slice cultures, Catherine Cohen-Solal for the preparation of acute hippocampal slices, and Nicolas Boulanger and Béatrice Loriod for the microarray study (genomic platform TAGC, Ibisa, INSERM U928). This study was supported by the French IRME and AFM Foundations, the ANR MALZ, and the FEDER PACA.

Received for publication July 24, 2010, and accepted in revised form April 27, 2011.

Address correspondence to: Emmanuel Nivet, Salk Institute for Biological Studies, 10010 North Torrey Pines Road, La Jolla, California 92037, USA. Phone: 858.453.4100, ext. 1324; Fax: 858.453.2573; E-mail: enivet@salk.edu.

Emmanuel Nivet's present address is: Salk Institute for Biological Studies, La Jolla, California, USA.

1. Maguire EA, et al. Navigation-related structural change in the hippocampi of taxi drivers. *Proc Natl Acad Sci U S A*. 2000;97(8):4398–4403.
2. Wiltrout C, Lang B, Yan Y, Dempsey RJ, Vemuganti R. Repairing brain after stroke: a review on post–ischemic neurogenesis. *Neurochem Int*. 2007; 50(7–8):1028–1041.
3. Jin K, et al. Increased hippocampal neurogenesis in Alzheimer's disease. *Proc Natl Acad Sci U S A*. 2004; 101(1):343–347.
4. Li B, et al. Failure of neuronal maturation in Alzheimer disease dentate gyrus. *J Neuropathol Exp Neurol*. 2008;67(1):78–84.
5. Lindvall O, Kokaia Z. Stem cells for the treatment of neurological disorders. *Nature*. 2006; 441(7097):1094–1096.
6. Yamasaki TR, Blurton-Jones M, Morrissette DA, Kitazawa M, Oddo S, LaFerla FM. Neural stem cells improve memory in an inducible mouse model of neuronal loss. *J Neurosci*. 2007;27(44):11925–11933.
7. Blurton-Jones M, et al. Neural stem cells improve cognition via BDNF in a transgenic model of Alzheimer disease. *Proc Natl Acad Sci U S A*. 2009; 106(32):13594–13599.
8. Qu T, Brannen CL, Kim HM, Sugaya K. Human neural stem cells improve cognitive function of aged brain. *Neuroreport*. 2001;12(6):1127–1132.
9. Acharya MM, et al. Rescue of radiation-induced cognitive impairment through cranial transplantation of human embryonic stem cells. *Proc Natl Acad Sci U S A*. 2009;106(45):19150–19155.
10. Bjorklund LM, et al. Embryonic stem cells develop into functional dopaminergic neurons after transplantation in a Parkinson rat model. *Proc Natl Acad Sci U S A*. 2002;99(4):2344–2349.
11. Martinez-Cerdeno V, et al. Embryonic MGE precursor cells grafted into adult rat striatum integrate and ameliorate motor symptoms in 6-OHDA-lesioned rats. *Cell Stem Cell*. 2010;6(3):238–250.
12. Freed CR, et al. Transplantation of embryonic dopamine neurons for severe Parkinson's disease. *N Engl J Med*. 2001;344(10):710–719.
13. Olanow CW, et al. A double-blind controlled trial of bilateral fetal nigral transplantation in Parkinson's disease. *Ann Neurol*. 2003;54(3):403–414.
14. Bachoud-Levi AC, et al. Effect of fetal neural transplants in patients with Huntington's disease 6 years after surgery: a long-term follow-up study. *Lancet Neurol*. 2006;5(4):303–309.
15. Murrell W, et al. Multipotent stem cells from adult olfactory mucosa. *Dev Dyn*. 2005;233(2):496–515.
16. Tome M, Lindsay SL, Riddell JS, Barnett SC. Identification of nonepithelial multipotent cells in the embryonic olfactory mucosa. *Stem Cells*. 2009; 27(9):2196–2208.
17. Delorme B, et al. The human nose harbors a niche of olfactory ectomesenchymal stem cells displaying neurogenic and osteogenic properties. *Stem Cells Dev*. 2010;19(6):853–866.
18. Lindsay SL, Riddell JS, Barnett SC. Olfactory mucosa for transplant-mediated repair: a complex tissue for a complex injury? *Glia*. 2010;58(2):125–134.
19. Shyu WC, et al. Implantation of olfactory ensheathing cells promotes neuroplasticity in murine models of stroke. *J Clin Invest*. 2008;118(7):2482–2495.
20. Kadar T, Dachir S, Shukitt-Hale B, Levy A. Sub-regional hippocampal vulnerability in various animal models leading to cognitive dysfunction. *J Neural Transm*. 1998;105(8–9):987–1004.
21. Grady MS, Charleston JS, Maris D, Witgen BM, Lifshitz J. Neuronal and glial cell number in the hippocampus after experimental traumatic brain injury: analysis by stereological estimation. *J Neurotrauma*. 2003;20(10):929–941.
22. Miller DB, O'Callaghan JP. Aging, stress and the hippocampus. *Ageing Res Rev*. 2005;4(2):123–140.
23. Bobinski M, et al. The histological validation of post mortem magnetic resonance imaging-determined hippocampal volume in Alzheimer's disease. *Neuroscience*. 2000;95(3):721–725.
24. Schmidt-Kastner R, Freund TF. Selective vulnerability of the hippocampus in brain ischemia. *Neuroscience*. 1991;40(3):599–636.
25. Feron F, et al. Autologous olfactory ensheathing cell transplantation in human spinal cord injury. *Brain*. 2005;128(pt 12):2951–2960.
26. Mackay-Sim A, et al. Autologous olfactory ensheathing cell transplantation in human paraplegia: a 3-year clinical trial. *Brain*. 2008;131(pt 9):2376–2386.
27. Rivera FJ, Sierralta WD, Minguell JJ, Aigner L. Adult hippocampus derived soluble factors induce a neuronal–like phenotype in mesenchymal stem cells. *Neurosci Lett*. 2006;406(1–2):49–54.
28. Jarrard LE. Use of excitotoxins to lesion the hippocampus: update. *Hippocampus*. 2002;12(3):405–414.
29. Roman FS, Marchetti E, Bouquerel A, Soumireu-Mourat B. The olfactory tubing maze: a new apparatus for studying learning and memory processes in mice. *J Neurosci Methods*. 2002;117(2):173–181.
30. Morris R. Developments of a water-maze procedure for studying spatial learning in the rat. *J Neurosci Methods*. 1984;11(1):47–60.
31. Leung CT, Coulombe PA, Reed RR. Contribution of olfactory neural stem cells to tissue maintenance and regeneration. *Nat Neurosci*. 2007;10(6):720–726.
32. Murrell W, et al. Olfactory mucosa is a potential source for autologous stem cell therapy for Parkinson's disease. *Stem Cells*. 2008;26(8):2183–2192.
33. Pandit SR, Sullivan JM, Egger V, Borecki AA, Oleskevich S. Functional effects of adult human olfactory stem cells on early–onset sensorineural hearing loss. *Stem Cells*. 2011;29(4):670–677.
34. Shetty AK, Rao MS, Hattiangady B. Behavior of hippocampal stem/progenitor cells following grafting into the injured aged hippocampus. *J Neurosci Res*. 2008;86(14):3062–3074.
35. Seidenfaden R, Desoeuvre A, Bosio A, Virard I, Cremer H. Glial conversion of SVZ–derived committed neuronal precursors after ectopic grafting into the adult brain. *Mol Cell Neurosci*. 2006;32(1–2):187–198.
36. Galea I, Bechmann I, Perry VH. What is immune privilege (not)? *Trends Immunol*. 2007;28(1):12–18.
37. Uccelli A, Moretta L, Pistoia V. Mesenchymal stem cells in health and disease. *Nat Rev Immunol*. 2008;8(9):726–736.
38. Munoz JR, Stoutenger BR, Robinson AP, Spees JL, Prockop DJ. Human stem/progenitor cells from bone marrow promote neurogenesis of endogenous neural stem cells in the hippocampus of mice. *Proc Natl Acad Sci U S A*. 2005;102(50):18171–18176.
39. Toni N, et al. Synapse formation on neurons born in the adult hippocampus. *Nat Neurosci*. 2007; 10(6):727–734.
40. Fox JM, Chamberlain G, Ashton BA, Middleton J. Recent advances into the understanding of mesenchymal stem cell trafficking. *Br J Haematol*. 2007;137(6):491–502.
41. Belema-Bedada F, Uchida S, Martire A, Kostin S, Braun T. Efficient homing of multipotent adult mesenchymal stem cells depends on FROUNT-mediated clustering of CCR2. *Cell Stem Cell*. 2008; 2(6):566–575.
42. Belmadani A, Tran PB, Ren D, Miller RJ. Chemokines regulate the migration of neural progenitors to sites of neuroinflammation. *J Neurosci*. 2006; 26(12):3182–3191.
43. Magge SN, et al. Role of monocyte chemoattractant protein-1 (MCP-1/CCL2) in migration of neural progenitor cells toward glial tumors. *J Neurosci Res*. 2009; 87(7):1547–1555.
44. Croitoru-Lamoury J, Lamoury FM, Zaunders JJ, Veas LA, Brew BJ. Human mesenchymal stem cells constitutively express chemokines and chemokine receptors that can be upregulated by cytokines, IFN-beta, and Copaxone. *J Interferon Cytokine Res*. 2007; 27(1):53–64.
45. Raheja LF, Genetos DC, Yellowley CE. Hypoxic osteocytes recruit human MSCs through an OPN/CD44-mediated pathway. *Biochem Biophys Res Commun*. 2008;366(4):1061–1066.
46. Yan YP, Lang BT, Vemuganti R, Dempsey RJ. Persistent migration of neuroblasts from the subventricular zone to the injured striatum mediated by osteopontin following intracerebral hemorrhage. *J Neurochem*. 2009;109(6):1624–1635.
47. Schraufstatter IU, Discipio RG, Zhao M, Khaldoyanidi SK. C3a and C5a are chemotactic factors for human mesenchymal stem cells, which cause prolonged ERK1/2 phosphorylation. *J Immunol*. 2009; 182(6):3827–3836.
48. Schmidt-Hieber C, Jonas P, Bischofberger J. Enhanced synaptic plasticity in newly generated granule cells of the adult hippocampus. *Nature*. 2004; 429(6988):184–187.
49. Wang S, Scott BW, Wojtowicz JM. Heterogenous properties of dentate granule neurons in the adult rat. *J Neurobiol*. 2000;42(2):248–257.
50. Bruel-Jungerman E, Rampon C, Laroche S. Adult hippocampal neurogenesis, synaptic plasticity and memory: facts and hypotheses. *Rev Neurosci*. 2007;

18(2):93–114.
51. Wernig M, et al. Functional integration of embryonic stem cell-derived neurons in vivo. *J Neurosci*. 2004;24(22):5258–5268.
52. Englund U, Bjorklund A, Wictorin K, Lindvall O, Kokaia M. Grafted neural stem cells develop into functional pyramidal neurons and integrate into host cortical circuitry. *Proc Natl Acad Sci U S A*. 2002; 99(26):17089–17094.
53. Hattiangady B, Rao MS, Zaman V, Shetty AK. Incorporation of embryonic CA3 cell grafts into the adult hippocampus at 4-months after injury: effects of combined neurotrophic supplementation and caspase inhibition. *Neuroscience*. 2006;139(4):1369–1383.
54. Hattiangady B, Shuai B, Cai J, Coksaygan T, Rao MS, Shetty AK. Increased dentate neurogenesis after grafting of glial restricted progenitors or neural stem cells in the aging hippocampus. *Stem Cells*. 2007;25(8):2104–2117.
55. Shetty AK, Zaman V, Hattiangady B. Repair of the injured adult hippocampus through graft-mediated modulation of the plasticity of the dentate gyrus in a rat model of temporal lobe epilepsy. *J Neurosci*. 2005;25(37):8391–8401.
56. Zaman V, Shetty AK. Fetal hippocampal CA3 cell grafts transplanted to lesioned CA3 region of the adult hippocampus exhibit long-term survival in a rat model of temporal lobe epilepsy. *Neurobiol Dis*. 2001;8(6):942–952.
57. Feron F, Perry C, McGrath JJ, Mackay-Sim A. New techniques for biopsy and culture of human olfactory epithelial neurons. *Arch Otolaryngol Head Neck Surg*. 1998;124(8):861–866.
58. Stoppini L, Buchs PA, Muller D. A simple method for organotypic cultures of nervous tissue. *J Neurosci Methods*. 1991;37(2):173–182.